

Desiccation cracks in saturated fine-grained soils: particle-level phenomena and effective-stress analysis

H. SHIN* and J. C. SANTAMARINA†

The formation of desiccation cracks in soils is often interpreted in terms of tensile strength. However, this mechanistic model disregards the cohesionless, effective-stress-dependent frictional behaviour of fine-grained soils. An alternative theory is explored using analyses, numerical simulations based on an effective-stress formulation, and experiments monitored using high-resolution time-lapsed photography. Results show that desiccation cracks in fine-grained sediments initiate as the air–water interface invades the saturated medium, driven by the increase in suction. Thereafter, the interfacial membrane causes an increase in the local void ratio at the tip, the air-entry value decreases, the air–water interface advances into the tip and the crack grows. The effective stress remains in compression everywhere in the soil mass, including at the tip of the desiccation crack. This crack-growing mechanism can explain various observations related to desiccation crack formation in fine-grained soils, including the effects of pore fluid salt concentration, slower crack propagation velocity and right angle realignment while approaching a pre-existing crack, and the apparent strength and failure mode observed in fine-grained soils subjected to tension. Additional research is required to develop a complementary phenomenological model for desiccation crack formation in coarse-grained sediments.

KEYWORDS: clays; failure; suction; theoretical analysis

La formation de fissures de dessèchement dans des sols est souvent interprétée sur le plan de sa résistance à la rupture. Cependant ce modèle mécanique ne tient pas compte du comportement de frottement sans cohésion, tribulaire de la tension efficace, des sols à grains fins. On examine une autre théorie faisant usage d'analyses, de simulations numériques basées sur une formulation à tension efficace, et d'expériences contrôlées avec la photographie temporisée à haute résolution. Les résultats montrent que les fissures de dessèchement dans des sédiments à grains fins se déclarent lorsque l'interface air–eau pénètre dans le milieu saturé, sous l'effet d'une augmentation de l'aspiration. Par la suite, la membrane interfaciale engendre une augmentation de l'indice de vide à la pointe, la valeur d'entrée de l'air diminue, l'interface air–eau avance dans la pointe, et la fissure s'agrandit. La tension efficace reste sous compression partout dans la masse du sol, y compris à la pointe de la fissure de dessèchement. Le mécanisme de formation de fissures peut expliquer différentes observations relative à la formation de fissures de dessèchement dans des sols à grains fins, y compris les effets de la concentration de sels de fluides interstitiels, la vitesse inférieure de propagation des fissures, et l'alignement perpendiculaire lorsqu'on s'approche d'une fissure préexistante, ainsi que le mode de résistance et de rupture apparent relevé dans des sols à grains fins soumis à des tensions. On doit poursuivre les recherches afin de développer un modèle phénoménologique supplémentaire pour la formation de fissures de dessèchement dans des sédiments à grains grossiers.

INTRODUCTION

The development of desiccation cracks damages geotechnical structures, exacerbates geo-environmental problems (e.g. fast flow path for contaminants), triggers instabilities and hinders the serviceability of earth structures. Desiccation cracks are important in other fields as well, from concrete technology (Lura *et al.*, 2007) to thin film formation and gels (Brinker & Scherer, 1990; Holmes *et al.*, 2006).

It is often assumed that soils crack when the tensile stress that develops within the soil mass exceeds the soil tensile strength, typically in the context of non-uniform drying or boundary-restrained free shrinkage. However, this mechanistic interpretation fails to recognise the inherent, cohesionless-yet-frictional effective-stress-dependent behaviour of soils. Furthermore, assumptions such as zero effective stress at the crack tip may not necessarily reflect the underlying particle-level mechanisms.

The purpose of this study is to develop a fundamental

understanding of crack initiation and propagation in granular materials by combining particle-level and macro-scale perspectives. At the particle level, the analysis centres on the tensile membrane at the water–air interface as it invades the soil driven by the increase in suction that accompanies water evaporation. At the macro-scale, the study explores changes in effective stress and volume near imperfections and crack tips. Together, these two perspectives provide a new understanding of desiccation crack formation in soils. The research methodology is described next; relevant references and previous studies are cited in each section.

RESEARCH METHODOLOGY

The study of desiccation crack initiation and propagation is herein implemented using a combination of experimental and numerical methods. The full scope of the experimental study involved 273 tests for different sediments, thickness, pore fluid chemistry and evaporation boundary condition. All results are adequately explained within the conceptual framework discussed in this study; for clarity and conciseness, the manuscript follows a series of desiccation experiments that involves slurries prepared by mixing Ca-montmorillonite (Panther Creek passing sieve #150; liquid limit = 97%; plastic limit = 47%) and deionised water at an initial water content of 150%. These mixtures are extensively mixed to

Manuscript received 4 February 2008; revised manuscript accepted 4 November 2010. Published online ahead of print 13 July 2011.

Discussion on this paper closes on 1 April 2012, for further details see p. ii.

* School of Civil and Environmental Engineering, University of Ulsan, Ulsan, Republic of Korea.

† Civil and Environmental Engineering, Georgia Institute of Technology, Atlanta, GA, USA.

form a homogeneous, low-viscosity slurry. Desiccation tests are conducted within a chamber with controlled temperature ($T = 25^{\circ}\text{C}$) and moisture conditions ($\text{RH} = 35\%$).

Two specimens are tested for each condition. One sits under an optical microscope (Leica MZ6) augmented with a digital camera (Qimaging) to obtain a $0.8\text{--}5\ \mu\text{m}/\text{pixel}$ resolution. In this case, images are gathered every 10 s. This test configuration is designed to obtain detailed information on crack initiation and propagation mechanisms. The second specimen sits on a scale (Pinnacle 6001 with 1 mg resolution) and its surface is photographed using a digital camera operating in time-lapse mode (Nikon Coolpix P4; 3264×2448 pixels; resolution $0.013\ \text{mm}/\text{pixel}$; photograph every 1 min). This test configuration provides the evolution of moisture, vertical and horizontal surface deformations, crack propagation, and the development of crack patterns (Matlab code modified from UraPIV – see <http://urapiv.wordpress.com> for further details; image processing details are discussed later in the text).

Analogous numerical simulations are run to gain additional information not attainable through experimentation. In these simulations, the soil mass is represented using the modified Cam Clay model, within an effective-stress analysis. Zero soil cohesion is assumed in all cases. Constitutive

model parameters and numerical simulation details including boundary conditions are summarised in Table 1.

STAGES IN DESICCATION CRACK FORMATION – STUDIES

Published desiccation crack initiation theories in soils and gels are summarised in Table 2. Presently, these theories are either incomplete or cannot be justified from the fundamental behaviour of uncemented granular materials. In this section a physically acceptable and complete mechanism is sought, and the different stages in desiccation crack formation are explored using the experimental and numerical tools described above.

Water evaporation and surface settlement before crack initiation

At the beginning, the supernatant water evaporates at an approximately constant rate. The effective stress in the soil is constant and the soil experiences no strain. Once the air–water interface reaches the soil surface, both continue moving downwards together. The soil skeleton consolidates owing to the increase in effective stress that equals the increase in

Table 1. Numerical study: model and material parameters

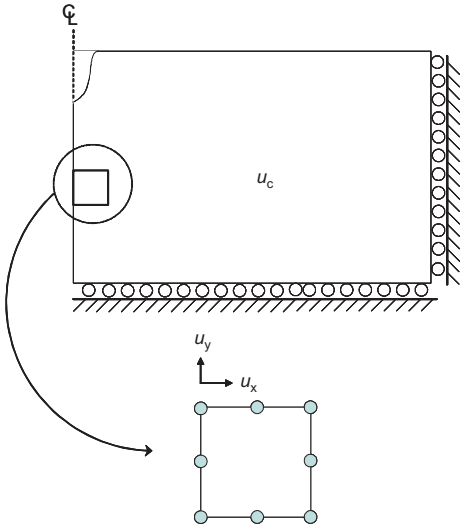
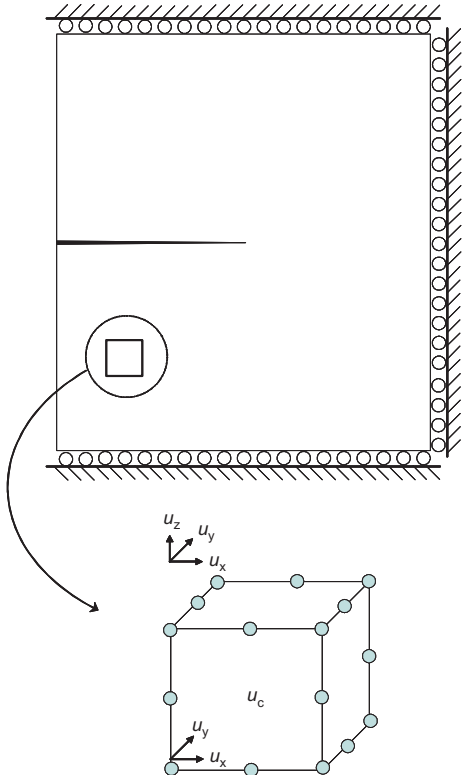
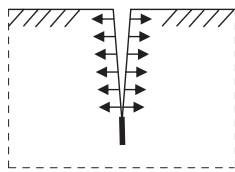
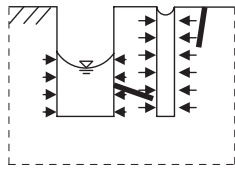
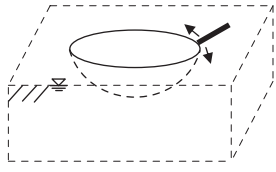
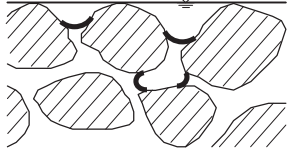
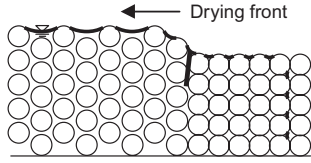
Element type and boundary conditions	
<p>(a) Study reported in Fig. 3 and Fig. 12 Element type: eight-node, axisymmetric or plane strain No friction against boundaries</p> 	<p>(b) Study reported in Figs 5, 6 and 11 Element type: 20-node, three-dimensional element No friction against boundaries</p> 
<p>Material properties: Constitutive model: Modified Cam Clay model with associated flow rule Soil properties: normally consolidated, compression index $C_c = 0.46$, swelling index $C_s = 0.15$, void ratio at 1 kPa, $e_{1\text{kPa}} = 3$, failure stress ratio $M_f = 1.0$, Poisson's ratio $\nu = 0.3$ Effective stress formulation with internal capillary suction u_c</p>	

Table 2. Previous theories for crack initiation in granular materials

Theory		Mechanism (selected references)
Tensile failure		Tensile stress > material tensile strength. Most commonly assumed model (Lachenbruch, 1962; Allen, 1982; Morris <i>et al.</i> , 1992; Naser Abu-Hejleh & Znidarcic, 1995; Konrad & Ayad, 1997; Hallett & Newson, 2005)
Irregular drying front		Difference in capillary pressures and subsequent failure of pore walls Conceptual – no verification (Zarzycki <i>et al.</i> , 1982)
Circumferential tension		Growth of radial crack due to hoop tension Conceptual – no verification (Scherer, 1990)
Air entry		Menisci invasion due to increasing capillary tension Conceptual – no verification (Childs, 1969; Brinker & Scherer, 1990; Herrera <i>et al.</i> , 2007)
Packing collapse		Collapse of particle layers by capillary suction Concept used to explain desiccation cracks in a drying strip (Holmes <i>et al.</i> , 2006)

suction u_c . The instantaneous void ratio e is related to u_c as prescribed in the one-dimensional normal consolidation line NCL: $e = e_{1\text{kPa}} - \lambda \ln(u_c/1 \text{ kPa})$.

This early stage of desiccation is first explored experimentally. A thin layer of fully saturated Ca-montmorillonite slurry (initial water content 150% – compared to $w_{LL} = 97\%$) is placed in a plastic container (diameter = 87 mm; wall height = 12 mm); the thin layer thickness, 1.9 mm, leads to a dense fracture pattern and increases the probability of fractures forming within the small observation zone. The vertical and horizontal displacements of a point on the soil surface can be computed from optical images with reference to an external fixed point taken as the image focus. Consider only those cracks that propagate towards the reference point; for a given pixel:

- the radial movement towards the image focus is used to compute the vertical displacement – Pythagorean analysis
- the horizontal displacement normal to the direction of crack propagation is determined from the tangential component of the pixel displacement. The evolution of the slurry water content and soil surface displacements are shown in Fig. 1. The quasi-constant rate of the evaporation stage coincides with continuous vertical settlement (i.e. the soil remains saturated – see also Bronswijk, 1988), and there is no lateral displacement.

The evolution of soil suction during drying is measured using the filter paper method (Bulut *et al.*, 2001). Slurry is poured into 30 containers and left to dry. At selected times,

specimens are sealed with a wet filter paper inside the container for 5 days. Then, the soil matric suction is determined from the water content in the filter paper using the drying filter paper calibration curve in Bulut *et al.* (2001). Data, superimposed on Fig 1, show that the constant rate of evaporation coincides with low levels of suction.

The increase in effective stress causes the increase in skeleton stiffness as well. From critical state, the one-dimensional constrained modulus M (kPa) can be related to suction u_c as

$$M = \frac{(1 + e_0) u_c}{\lambda} \quad \text{before air entry} \quad (1)$$

where e_0 is the initial void ratio. Therefore, low suction during early stages of evaporation implies low skeletal stiffness. Eventually, further evaporation and increased suction will force the air–water interface membrane to invade the soil mass. This situation is analysed next.

Crack initiation

Cracks initiate during the constant rate of evaporation stage in all tests conducted as part of this study (such as in Fig. 1). The soil is still fully saturated at crack initiation, that is the air–water interface and the apparent soil surface coincide (in agreement with observations based on gels by Brinker & Scherer, 1990). The soil surface experiences no horizontal displacement before crack initiation, and limited vertical movement thereafter (Fig. 1).

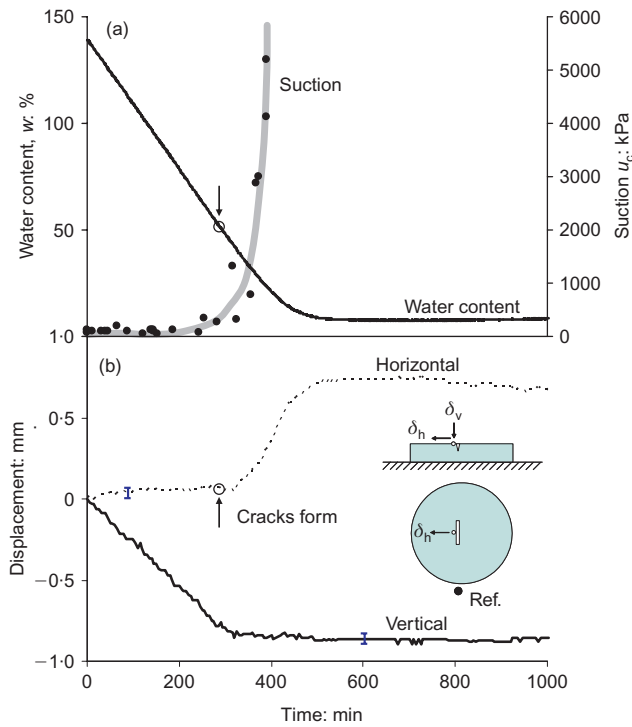


Fig. 1. Desiccation plotted against time. (a) Water content and suction evolution. (b) Vertical settlement and horizontal displacement of a point on the soil surface next to a developing desiccation crack. The segments indicate the displacement resolution range from image analysis

The relevance of surface defects. In particular, all the current study's experimental observations with homogeneous fine-grained slurries show that crack initiation always takes place at surface defects, such as sub-millimetre size 'craters', and propagate both laterally and downward (Fig. 2 – see also Allen (1982)). Inclusions, large aggregate anomalies or small topographic features (e.g. indentations) can trigger crack formation owing to shrinkage distortion of the surrounding medium (see also Townner (1988), Zabat *et al.* (1997) and Weinberger (1999)).

Void ratio at the tip and in the far field. Furthermore, cracks always start at the bottom of the defect, not at the equator (Fig. 2 – contrary to Scherer (1990)). A numerical simulation is conducted to investigate the underlying effective-stress mechanisms. A Gaussian-shaped surface defect is considered in a modified Cam Clay material, and modelled using an axisymmetric mesh (model parameters, mesh details and boundary conditions are summarised in Table 1, column (a)). Internal suction is applied throughout the whole medium, starting at an equilibrium condition $p' = 0.01$ kPa with homogeneous void ratio $e = 3.92$, and gradually increasing the suction to reach $p' = 100$ kPa with far-field void ratio $e = 2.105$. Fig. 3(a) shows the void ratio distribution around the defect. Consolidation takes place everywhere; however, a higher void ratio is reached at the tip of defects than anywhere else, particularly in narrow defects: the $e-\sigma'$ path at the tip gradually deviates from the $e-\sigma'$ path in the far field, which follows the normal consolidation line NCL (Fig. 4).

Air entry line $e-u_c$ (AEL – particle-scale analysis). A lower air-entry suction u_c^{AE} (kPa) corresponds to a higher local void ratio e . A particle-scale analysis allow the estimation of the air-entry suction assuming parallel platy particles of thickness

t separated at a distance d (Fig. 3(b)): the void ratio is $e = d/t$, and the specific surface is $S_s = 2/(\rho t)$. Then, the air-entry suction $u_c^{AE} = 2T_s/d$ (Laplace equation) is

$$u_c^{AE} = \frac{\rho T_s S_s}{e} \quad (2)$$

where ρ (g/cm^3) is the mass density of the particle and $T_s = 0.072$ N/m is surface tension of water. A similar analysis for lower specific surface grains can be made in terms of spherical particles with radius R

$$u_c^{AE} = \frac{2 T_s / R}{\sqrt[3]{\frac{2}{3} \pi (1 + e) - 1}} \quad (3)$$

The change in air entry suction u_c^{AE} with void ratio e defines the air-entry line AEL in the void-stress space. These two particle-scale equations are written in terms of macro-scale parameters S_s and e to gain insight into the interplay among governing parameters.

Crack initiation at air invasion. The void ratio at the tip reaches the AEL first, and air invades the soil mass at the tip while the rest of the soil remains saturated (Fig. 4). This is the moment when the crack initiates (see also Childs (1969)); further crack development will require the ability of particles to displace. This sequence of events is in agreement with all the present authors' experimental observations that place crack initiation at the tip of defects in soft, fine-grained sediments (Note: the complete mechanistic description of crack initiation and propagation is presented in the section later entitled 'Stages in desiccation crack formation – summary').

Fine as opposed to coarse-grained soils. Soft, high-specific-surface soils (typically made of platy particles) have small pores so that the AEL intersects the NCL at high suction (Fig. 4). Air invasion causes large particle displacements and crack opening because of the low soil stiffness (see Prodanovic & Bryant (2006) and Jain & Juanes (2008) for particle forces induced by interfacial tension in the context of methane hydrates). On the other hand, coarse low-specific-surface soils have large pores, low air-entry values, steep AEL and high skeletal stiffness (flat NCL). Therefore, there are almost no differences in air entry at tips or anywhere else, and the interfacial water–air membrane massively invades the soil.

Summary. The increased local void ratio at the tip of defects facilitates air–water membrane invasion into the soil mass as suction increases in a drying soil. Air invasion is the starting point for desiccation crack formation in saturated soft soils.

Crack propagation

Analogous to crack initiation, it may be anticipated that the void ratio increases and the air-entry value decreases at the crack tip, the air–water membrane preferentially invades the soil at the tip and the crack propagates.

This growth mechanism is tested next by modelling a homogeneous single-layer slab of soil, subjected to homogeneous suction $u_c = 100$ kPa in equilibrium at a void ratio $e = 2.087$. (Note that neither plane strain nor plane stress conditions can be used to simulate this condition – simulation details are given in Table 1, column (b).) After equilibrium, the three vertical nodes at the centre of the left

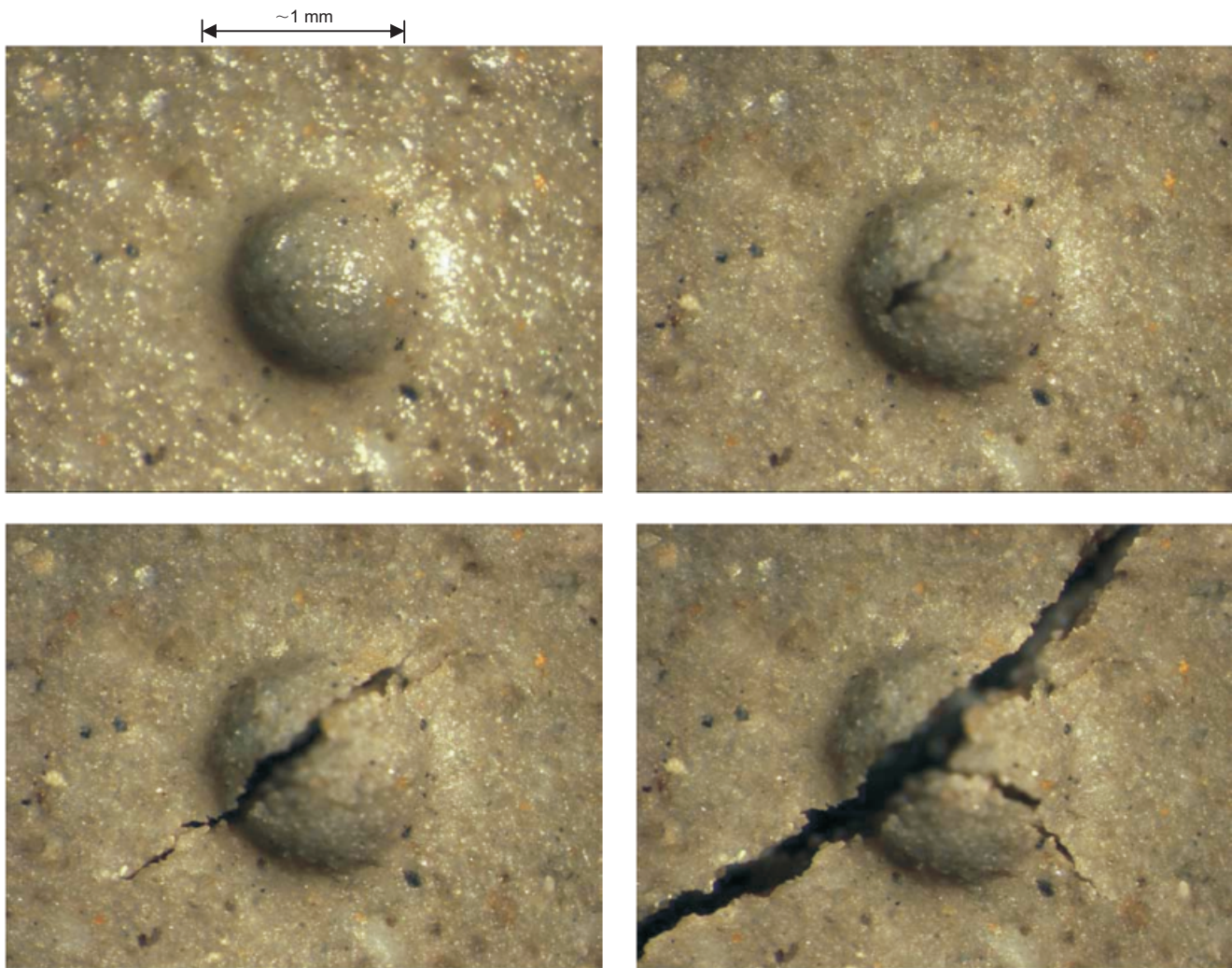


Fig. 2. Crack initiation at the bottom of a surface defect during evaporation. This defect originated as a surface-trapped gas bubble

boundary are simultaneously released to emulate crack initiation while suction is kept constant (initiation point A in Fig. 5). To prevent numerical instability, node forces are gradually released while the soil mass regains equilibrium under constant suction. In agreement with results in Fig. 1, the sediment is considered at the verge of air entry at $u_c \approx 100$ kPa; then, a new set of three vertical nodes is released where the local void ratio is highest. The process is repeated to reproduce crack growth. Fluid pressure homogenisation may not be reached throughout the medium during crack propagation in real systems; however, the time for significant pressure diffusion at the tip is short given the short length scale involved.

Instantaneous stress–volume data are shown in Fig. 5. The crack propagates along the centreline. There is a marked drop in effective horizontal stress immediately ahead of the crack tip; then, the horizontal effective stress recovers to the applied suction after the crack passes. The void ratio at the crack tip is higher than anywhere else. The soil next to the crack walls behind the tip reconsolidates and the void ratio decreases owing to the compression imposed by capillary suction against the crack walls (Figs 5(b) and 5(c)).

The numerical simulation approach is validated by comparing numerical predictions against experimental observations. Displacements transverse δ_y and parallel δ_x to the propagation direction x are determined using digital image correlation between consecutive microphotographs, when the crack is at beginning position B and at the end position E.

Nodal displacements are readily obtained from the corresponding stages in the numerical simulation. A strong resemblance is observed between experimental and numerical results (Fig. 6). There is a quasi-circular shape of the transverse displacement δ_y bulb, which expands behind the crack tip as the crack opens during suction-driven consolidation; the affected region scales with the propagation distance. No transverse movement is observed ahead of the crack, except in the far field. The displacement parallel to the direction of crack propagation δ_x is towards the tip, both behind and ahead of the crack tip.

Results in Fig. 5 (and Fig. 6) confirm that the soil dilates ahead of the tip, the air-entry suction decreases at the tip and the soil becomes reconsolidated as the crack advances further. It is important to highlight that membrane invasion and crack propagation take place while the effective-stress state is in compression everywhere in the medium including at the crack tip. (Note: Holmes *et al.* (2006) make a similar observation in a study with alumina suspensions.)

STAGES IN DESICCATION CRACK FORMATION – SUMMARY

On the bases of previous experimental observations and numerical results, the following stages in desiccation crack initiation and growth in saturated fine-grained soils are identified (Fig. 7).

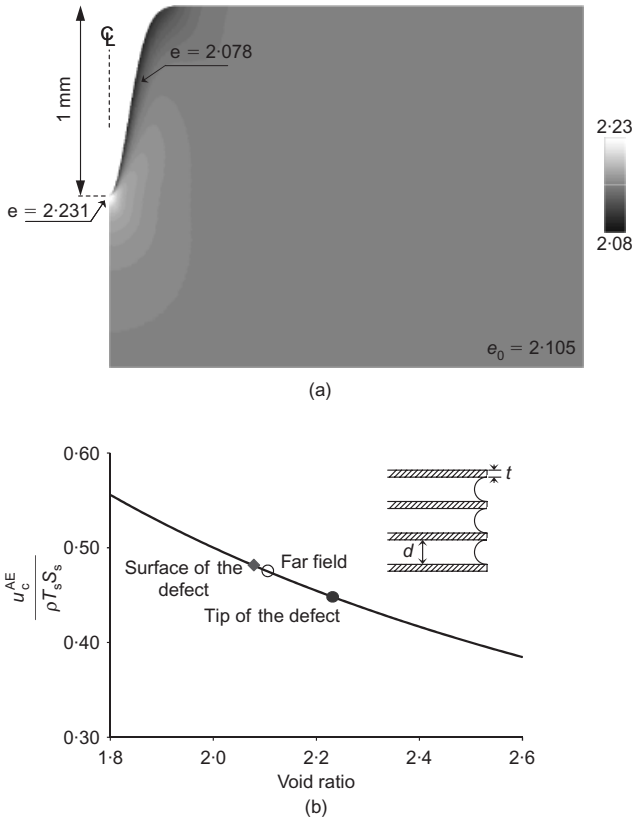


Fig. 3. Surface defects and crack initiation. Local void ratio evolution during desiccation – finite-element analysis. The domain size is 6 mm × 6 mm, and the defect depth is 1 mm. (a) Void ratio when suction $u_c = 100$ kPa. Model details in Table 1, column (a). (b) Required suction for air entry at the tip and on the surface as a function of the local void ratios – equation (2)

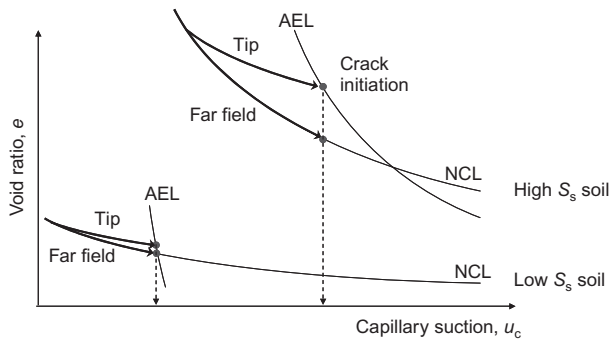


Fig. 4. The air-entry line AEL and the normal consolidation line NCL. Trends are shown for soft high-specific-surface soils such as NC clays and for stiff low-specific-surface soils such as sands. Air-entry lines are defined by equations (2) and (3). Both NCLs defined as $e = e_{1kPa} - \lambda \ln(u_c/1 \text{ kPa})$

Water surface above the sediment surface. In this stage, the water evaporates freely, the pore fluid pressure is positive everywhere inside the sediment, and there is no capillary suction (Fig. 7(a)). Eventually, the water level reaches the sediment surface (Fig. 7(b)); at this instant, the pore fluid pressure on the surface is zero.

Mobilisation of tensile membrane and development of suction. Further evaporation brings the air–water interface membrane against grain surfaces and other topographic features (Fig. 7(c)). The membrane grabs on to soil particles and resists invading the soil. Capillary suction develops in the

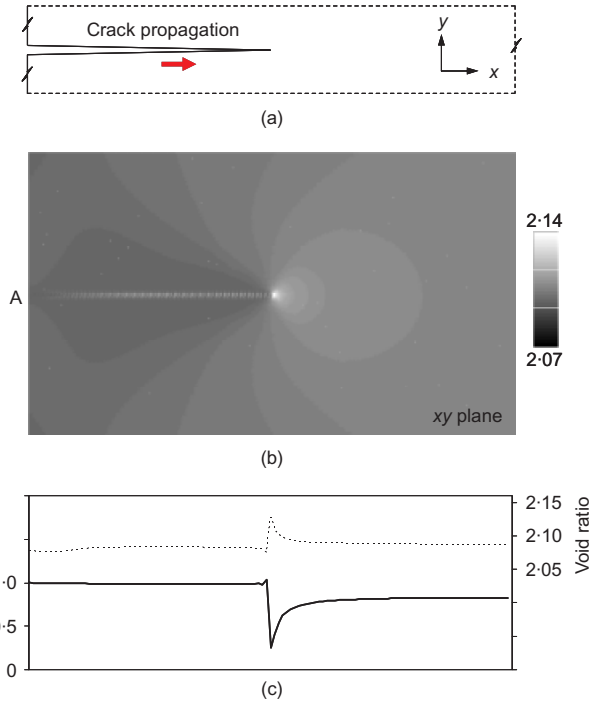


Fig. 5. Void ratio evolution during crack propagation: (a) geometry and crack tip location; (b) void ratio contours – view on xy plane normal to the xz crack plane; (c) effective stress σ'_v normal to the crack plane and void ratio along the crack alignment. Model details in Table 1, column (b) – plane stress with suction u_c . The simulated domain size is 12 mm long and 14 mm wide (full length shown)

pore fluid (Laplace’s equation) and effective stress in the granular skeleton. The soil consolidates, the skeletal stiffness gradually increases and the magnitude of the vertical one-dimensional settlement is equal to the amount of water that evaporates. The soil remains saturated throughout this stage.

Membrane invasion – crack initiation. The increased stiffness of the soil skeleton hinders further consolidation. If evaporation continues, capillary suction causes the air–water interface to invade the sediment. Air intrusion starts at the largest pores, often associated with surface defects. Membrane invasion causes particle displacement into the soil mass, normal to and away from the air–water interface. Therefore, membrane invasion takes place at surface features following the order prescribed by pore size and particle mobility. The pore size increases at the tip of the invading front so that further membrane invasion is favoured at the tip, signalling crack initiation (Fig. 7(d)). Crack initiation can be expected during the constant rate of evaporation regime (Fig. 7 – see also Fig. 1).

Vapour transport away from the soil surface becomes increasingly more difficult as the air–water interface is pulled into the soil. Then, the evaporation rate decreases almost linearly as the total suction increases (Fig. 1 – Brinker & Scherer (1990) – see also Wilson *et al.* (1997) but in linear–linear scale).

Crack propagation. Crack growth consists of membrane invasion into the enlarged pores at crack tips, where the void ratio increases and the air-entry value decreases. Once the air–water interface membrane invades ahead of the crack tip, a new surface is formed and the process repeats itself. Particle mobility and changes in void ratio decrease with

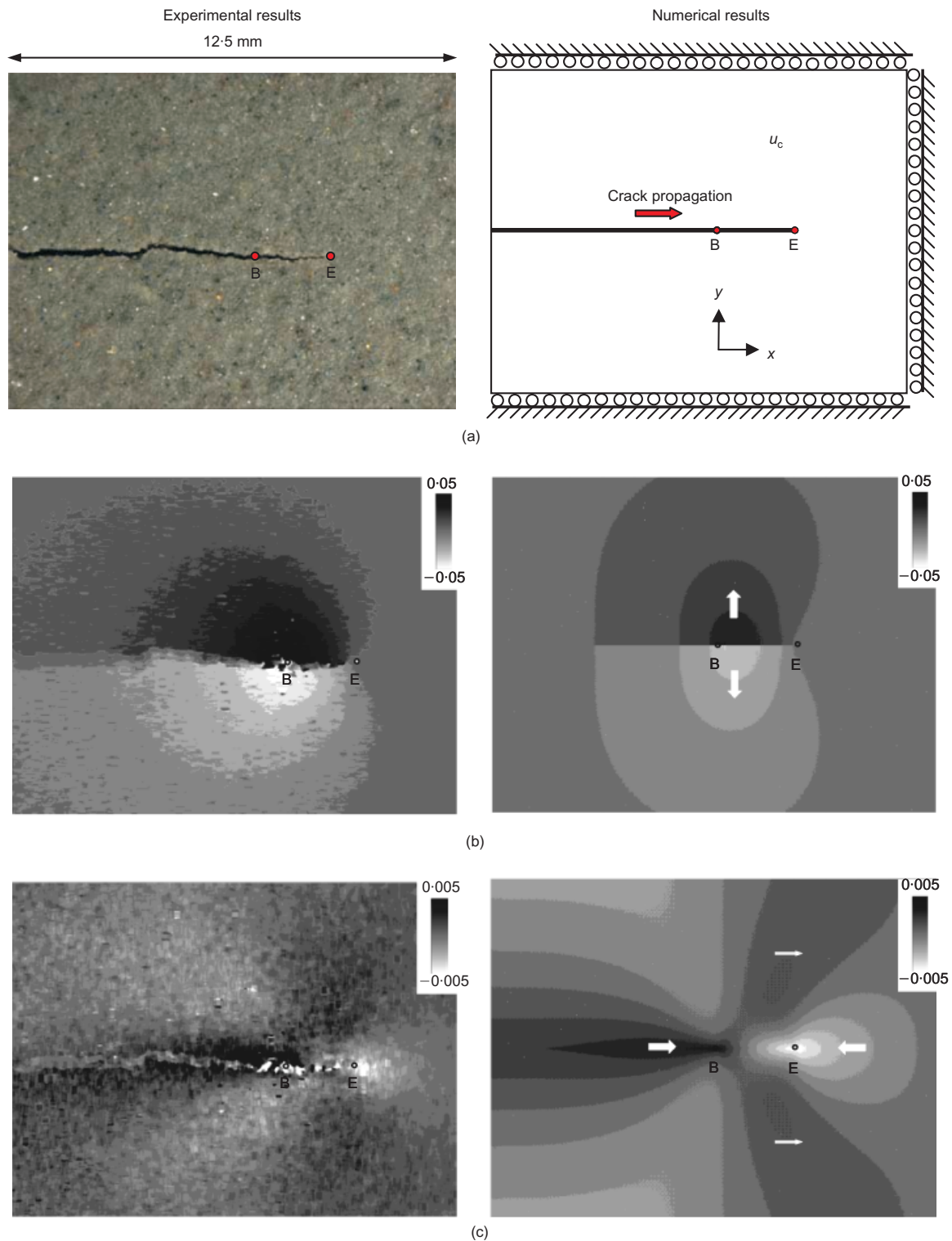


Fig. 6. Displacement fields associated with a crack propagating from a beginning point B to the end point E. Comparison between experimental and numerical displacements: (a) photograph and finite-element method model; (b) displacement δ_y (mm) normal to the crack plane; (c) displacement δ_x (mm) parallel to the crack propagation alignment. Soil: Ca-montmorillonite; initial water content $w = 150\%$. Numerical simulation details in Table 1, column (b) – plane stress with suction u_c . The simulated domain size is 12 mm long and 14 mm wide (full length shown)

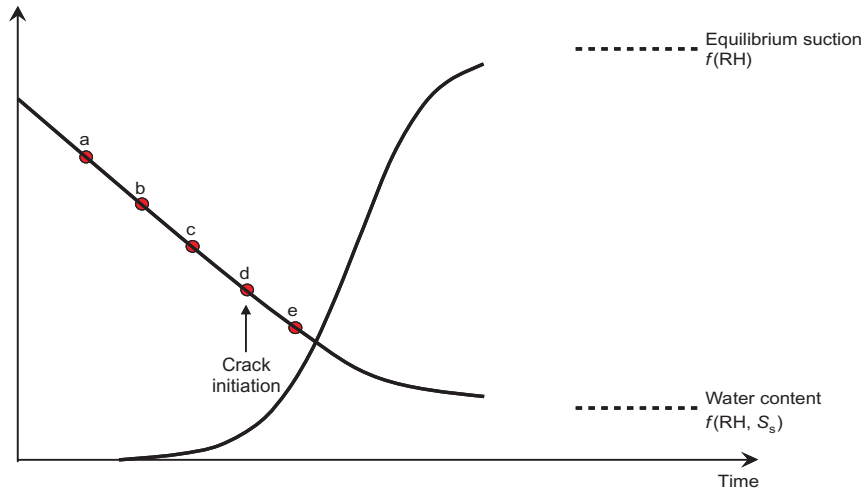
depth, so that preferential membrane invasion takes place into lateral pores, and cracks propagate along the surface. Once again, the soil mass experiences compressive effective stress everywhere and at all times during the desiccation-crack process.

Eventually, the soil mass between cracks becomes unsaturated. The long-term equilibrium capillary suction reflects the relative humidity, and water content is the retention

capacity of the soil as determined by its specific surface and the prevailing relative humidity.

FURTHER ANALYSES – DISCUSSION

The proposed sequence of events for desiccation crack initiation and growth in saturated fine-grained soils is inherently compatible with the frictional, effective-stress-dependent



Stages	(a)	(b)	(c)	(d)	(e)
Global view					
Particle scale view					
Comments	Evaporation of supernatant water No suction No strain in the soil skeleton	Air-water interface membrane reaches the soil surface	Membrane forms around soil particles Suction increases Consolidation of soil skeleton and increase in stiffness	Air invades the largest pores The air-water interface membrane pushes particles away from the invaded pore Pore size increase at the tip and crack grows	Crack propagation and formation of polygons Vertical deformation ceases Eventually, the soil mass becomes unsaturated

Fig. 7. Water evaporation, soil desiccation and crack formation – summary of pore and particle scale processes

behaviour of soils. In this section, the hypothesised mechanism is invoked to explain other observations related to desiccation crack formation in soils.

Desiccation cracks, pore size distribution and soil fabric

It follows from the previous discussion that membrane invasion and crack initiation will more readily take place in soils with non-uniform pore size distribution than in soils of similar porosity but uniform pore size. Furthermore, sediments with initial mono-size pores may develop a bimodal

distribution as suction increases (Koliji *et al.*, 2006). Assuming log-normal pore size distribution, the ratio between standard deviation s_d and mean μ is typically between 0.3 and 0.7. Air will invade the largest pores first, and the air-entry line will plot at lower levels of suction than those predicted by equations (2) or (3).

Pore size distribution, fabric, and stiffness in fine-grained minerals are determined by the pore fluid ionic concentration, permittivity and pH (Palomino & Santamarina, 2005; Zabot *et al.*, 1997). In particular, fine-grained soils mixed with a high-concentration salt solution form aggregated

fabrics and exhibit larger pore diameters than dispersed fabrics at the same confining stress (Wang & Xu, 2007). Therefore, the pore fluid chemistry may affect desiccation crack formation. Indeed, slurries containing aggregations developed a more extensive fracture network than slurries made of dispersed grains (van Damme & Ben Ohoud, 1990; Zabat *et al.*, 1997).

The role of ionic concentration on fabric formation and desiccation cracks is confirmed by conducting desiccation tests with two sodium (Na)–bentonite slurries prepared at the same initial water content of 1000%, one mixed with deionised water and the other with 0.1M NaCl (sodium chloride) (Note: the test procedure is identical to the calcium (Ca)–bentonite tests presented earlier). Results presented in Fig. 8 corroborate that the soil mass tends to remain monolithic for low-ionic-concentration pore fluids (dispersed fabric with small and uniform pore size). On the other hand, the soil with high-ionic-concentration pore fluid becomes extensively fractured as the air–water membrane readily invades the multiple large surface pores between aggregations.

Crack propagation near pre-existing cracks – crack pattern formation

Propagating contraction cracks in cohesive media turn towards existing cracks until they finally intersect at right angles (Morris *et al.*, 1992). Typically, this observation is explained by the maximum stress release criterion (Lachenbruch, 1962): since the internal stress normal to the existing crack plane has been released already, the propagating contraction crack will approach the pre-existing crack normal to it.

Furthermore, predictions based on linear elastic fracture mechanics in cohesive media show that as the crack tip approaches the free boundary, the stress intensity experiences a pronounced increase (Fig. 9), and the crack propagation velocity increases (experimental data for cohesive media in Dally *et al.* (1985)).

Multiple cases of desiccation crack tip propagation approaching earlier cracks in soils were measured, and results confirmed the well-known normal intersection. However, the

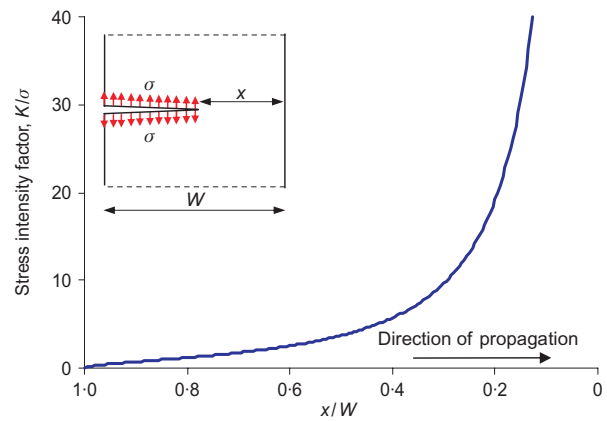


Fig. 9. Change in stress intensity factor as the crack approaches a free boundary (analytical solution in Sanford (2003)).

velocity of propagation decreases in *all cases* as the distance to the free boundary decreases (Fig. 10). Why do desiccation cracks in soils slow down and turn towards the nearby free boundary? One explanation consistent with the proposed mechanism is that the lower velocity results from delayed water migration into the expanding soil at the crack tip in the vicinity of the ‘effectively impervious free boundary’ at the existing crack face. Furthermore, suction acts at the free boundary, and increases the isotropic stress at the approaching crack tip; therefore there is a lower increase in void ratio and the air-entry value remains high.

This mechanical explanation is confirmed by the simulation of crack propagation towards a skewed free boundary shown in Fig. 11 (model details in Table 1, column (b) – nodes are released only along the central alignment in this simulation). There is restricted volume dilation at the crack tip near the free boundary as can be seen by the size of the void ratio bulbs in the three frames shown in Fig. 11. Furthermore, and contrary to results in Fig. 6, consolidation-induced displacements are much more pronounced on the right-hand side of the crack, that is closer to the free boundary (not shown here), driving void ratio changes, air

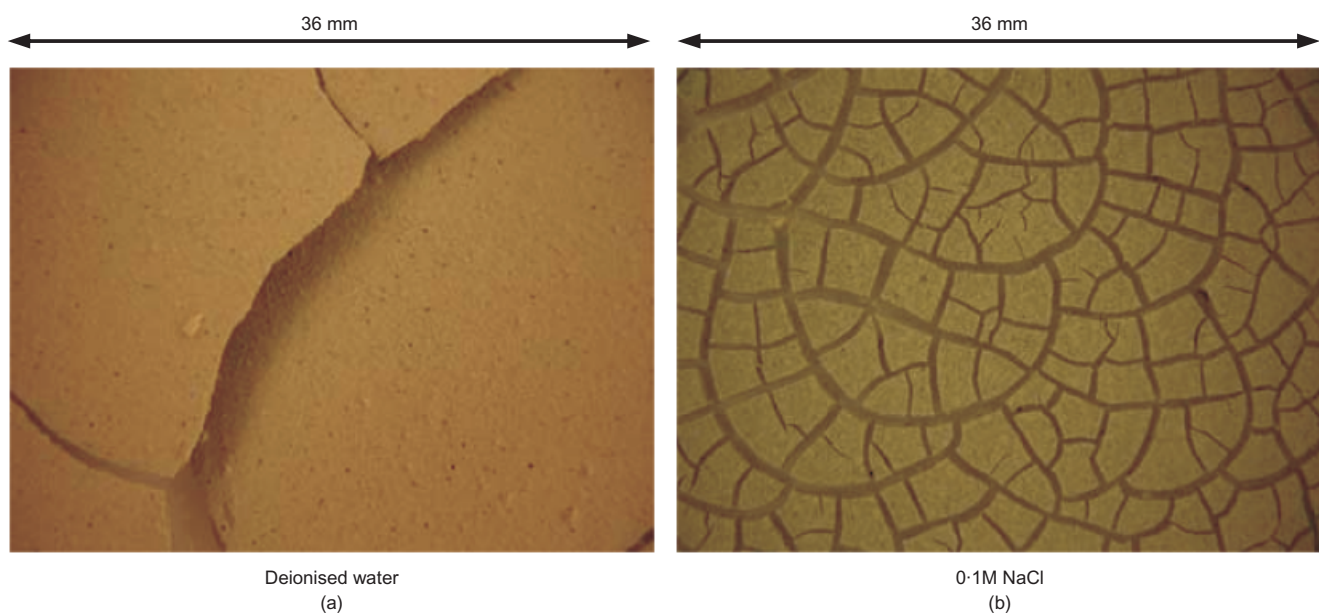


Fig. 8. Effect of salt concentration on desiccation crack pattern. Sodium (Na)–bentonite slurry prepared at an initial $w = 1000\%$. Pore fluid condition: (a) slurry mixed with deionised water; (b) slurry mixed with 0.1M sodium chloride (NaCl). Initial soil thickness is 2 mm in both tests

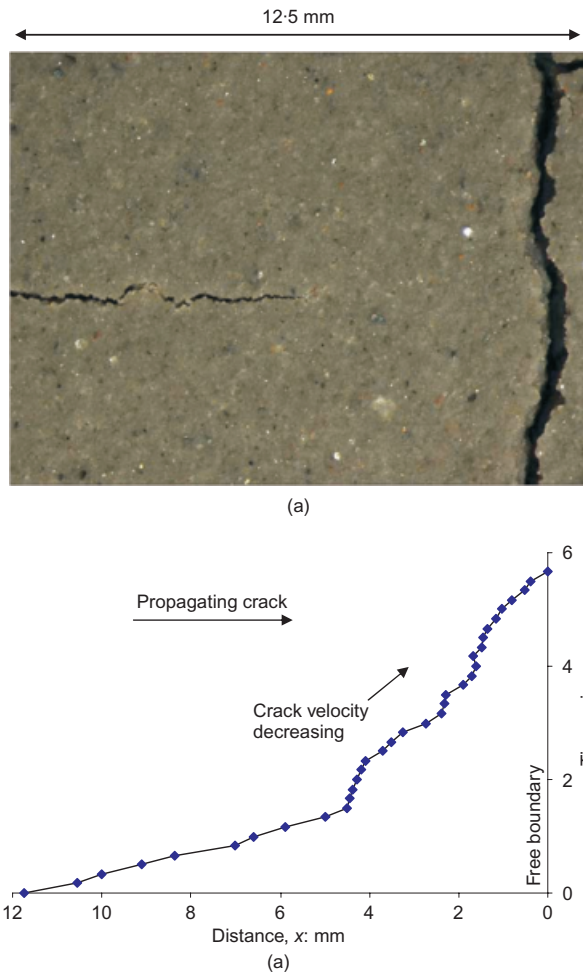


Fig. 10. Desiccation crack propagation towards an existing crack or free boundary. (a) Microphotograph of crack tip at a distance $x = 4.8$ mm from a pre-existing crack. (b) Crack tip propagation plotted against time. Soil: Ca–montmorillonite; initial water content $w = 150\%$

invasion and crack propagation normal to the pre-existing crack.

Tensile strength in fine-grained soils

The ‘apparent tensile strength’ exhibited by an uncemented saturated soil specimen in air cannot be justified on the bases of inter-particle electrical forces. In fact, strength must result from inter-granular friction and the confining effect of capillary suction that develops as the air–water interface resists intruding the saturated medium (a comprehensive experimental study with clay beams can be found in Thusyanthan *et al.* (2007); tensile tests in sandy sediments are presented in Lu *et al.* (2007)).

The failure of a saturated soil in tension is explored using numerical simulation. The soil is modelled as a modified Cam Clay material and an internal suction of 100 kPa is applied first (model details in Table 1, column (a)). After equilibrium, the specimen is subjected to 50 kPa tension. The void ratio and deviatoric stress fields are shown in Fig. 12. While the maximum deviatoric stress ratio develops at 45° from the crack tip, the void ratio expansion is aligned with the notch. Therefore, the air–water membrane will invade the specimen and the crack will grow normal to the applied tensile load, eventually giving the appearance of a tensile failure, while the soil mass has remained in compression at all times.

Based on the initial air-entry value u_0 , the upper bound for the apparent soil tensile strength can be estimated for the Mohr–Coulomb failure criterion (saturated soils)

$$\sigma_T \leq u_0 \frac{2 \sin(\phi')}{1 + \sin(\phi')} \quad \text{upper bound} \quad (4)$$

This is an upper bound because the void ratio increases and the air-entry value at the tip decreases during the tensile test, thus a lower ‘tensile strength’ will be measured (equation (2)).

Crack initiation in drying slurries occurs while the stress history at the tip is still normally consolidated. However, crack propagation away from the initial defect and in tensile tests in general cause effective stress unloading at the crack tip; this situation prompted Thusyanthan *et al.* (2007) to explore failure on the Hvorslev failure surface when the initial capillary suction is high.

Observations related to saturation – model limitations

The degree of saturation is extensively used in unsaturated soil mechanics (Fredlund & Rahardjo, 1995; Rodriguez *et al.*, 2007). However, this is a large-scale parameter and its utilisation requires careful interpretation in the context of desiccation cracks in fine-grained soils where soil blocks between cracks are expected to remain fully saturated long after crack formation, as can be inferred from Fig. 4 for the case of high-specific-surface soils. (Note: this statement could be experimentally confirmed only until early stages of fracture formation and propagation.)

In coarse-grained soils, the air-entry value is low, the skeletal stiffness is high and the air–water interfacial membrane readily invades the soil mass at relatively low suction (Fig. 4). Hence, a complementary phenomenological model for desiccation crack formation in coarse-grained sediments is required. Still, menisci at inter-particle contacts pull particles together (Cho & Santamarina, 2001; Chertkov *et al.*, 2004; Peng & Horn, 2007) and can cause contractive strains that lead to large-scale desiccation fractures such as giant desiccation cracks (see examples in Harris (2004)).

CONCLUSIONS

The total stress tensile strength criterion for desiccation crack formation hides the inherent cohesionless, effective-stress-dependent frictional strength of uncemented soils. The fundamental mechanism for desiccation crack initiation and growth in fine-grained sediments is centred on the air–water interface membrane. Initially the air–water interface membrane resists invading pores, capillary suction increases, the effective stress increases, the soil consolidates and the skeletal stiffness increases. Eventually, the air–water interface membrane invades the largest pores and causes particle displacement away from the invasion point. The void ratio increases at the tip and facilitates further membrane invasion and crack growth.

This sequence of events explains known observations related to desiccation crack formation in fine-grained soils, including: pore fluid and fabric effects on the desiccation crack pattern (due to pore size distribution and air entry); slower crack propagation velocity as the crack approaches the free boundary of a pre-existing crack (due to delayed water migration and a smaller reduction in air-entry value next to the free boundary); right angle junction in crack pattern formation (caused by the rotation of the void ratio expansion contours towards the pre-existing free boundary); and frictional resistance in axial extension yet with a normal failure surface (due to the increase in void ratio and

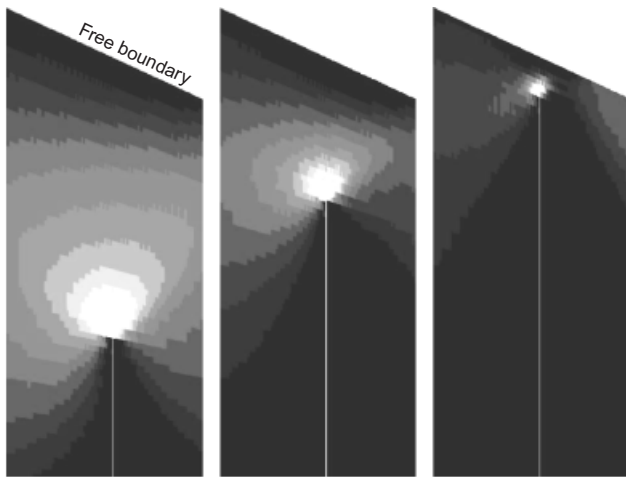


Fig. 11. Void ratio evolution as the crack advances and approaches a skewed free boundary. The highest void ratio develops at the crack tip (white, $e = 2.35$). The sediment consolidates along the crack behind the tip to reach $e = 2.05$ (shown as dark grey). Model details in Table 1, column (b) – plane stress with suction u_c . The simulation is 12 mm long and 10 mm wide; a 4 mm wide section of the simulated domain is shown

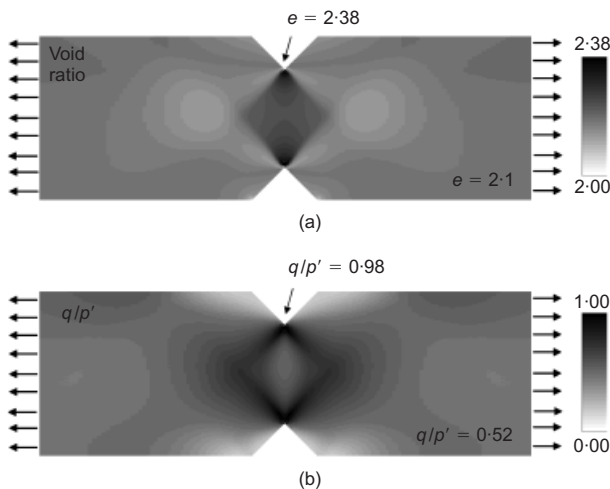


Fig. 12. Tensile test simulation. Initial suction $u_c = 100$ kPa. Condition when a tensile stress $\sigma = 50$ kPa is applied: (a) void ratio distribution; (b) deviatoric stress ratio q/p . Model details in Table 1, column (a)

membrane invasion normal to the applied extension). In all cases, membrane invasion and desiccation crack propagation take place while the state of effective stress remains in compression everywhere in the soil mass, including at the crack tip.

Additional research is required to develop a complementary phenomenological model for desiccation crack formation in coarse-grained sediments.

ACKNOWLEDGEMENTS

Support for this research was provided by the Goizueta Foundation and Department of Energy project on gas production from methane hydrates.

NOTATION

AEL	air-entry line
C_C	one-dimensional compression index (slope in e - $\log\sigma'$)
C_S	one-dimensional swelling index (slope in e - $\log\sigma'$)

d	separation distance between parallel platy particles
e	void ratio
e_0	initial void ratio
M	one-dimensional constrained modulus ($\Delta\epsilon_z/\Delta\sigma'_z$)
M_f	failure stress ratio
NCL	normal consolidation line
p'	mean effective stress
q	deviatoric stress
R	radius of spherical particle
RH	relative humidity
S_s	soil specific surface
s_d	standard deviation for the log-normal distribution of pore size
T_s	surface tension
t	thickness of platy particles
u_c	capillary suction
u_c^{AE}	air entry suction
w	water content
δ_x	displacement parallel to the direction of crack propagation
δ_y	displacement transverse to the direction of crack propagation
λ	one dimensional compression index
μ	mean pore size
ν	Poisson's ratio
ρ	mass density of the mineral that makes the particle
σ'	effective stress
σ_T	apparent tensile strength
ϕ	angle of internal shear strength

REFERENCES

- Allen, J. R. L. (1982). *Sedimentary structures, their character and physical basis*. Amsterdam: Elsevier.
- Brinker, C. J. & Scherer, G. W. (1990). *Sol-gel science: the physics and chemistry of sol-gel processing*. Boston: Academic Press.
- Bronswijk, J. J. B. (1988). Modeling of water balance, cracking and subsidence of clay soils. *J. Hydrol.* **97**, No. 3-4, 199-212.
- Bulut, R., Lytton, R. L. & Wray, W. K. (2001). Soil suction measurements by filter paper. In *Expansive clay soils and vegetative influence on shallow foundations*, pp. 243-261. Reston, Virginia: American Society of Civil Engineers.
- Chertkov, V. Y., Ravina, I. & Zadoenko, V. (2004). An approach for estimating the shrinkage geometry factor at a moisture content. *Soil Sci. Soc. Am. J.* **68**, No. 6, 1807-1817.
- Childs, E. C. (1969). *An introduction to the physical basis of soil water phenomena*. London: Wiley.
- Cho, G. C. & Santamarina, J. C. (2001). Unsaturated particulate materials – particle-level studies. *J. Geotech. Geoenviron. Engng* **127**, No. 1, 84-96.
- Dally, J. W., Fournay, W. L. & Irwin, G. R. (1985). On the uniqueness of the stress intensity factor-crack velocity relationship. *Int. J. Fracture* **27**, No. 3-4, 159-168.
- Fredlund, D. G. & Rahardjo, H. (1995). *Soil mechanics for unsaturated soils*. New York: Wiley.
- Hallett, P. D. & Newson, T. A. (2005). Describing soil crack formation using elastic-plastic fracture mechanics. *Eur. J. Soil Sci.* **56**, No. 1, 31-38.
- Harris, R. C. (2004). *Giant desiccation cracks in Arizona*, OFR 04-01. Tucson: Arizona Geological Survey.
- Herrera, M. C., Lizcano, A. & Santamarina, J. C. (2007). Colombian volcanic ash soils. In *Characterization and engineering properties of natural soils* (eds T. S. Tan, K. K. Phoon, D. W. Hight and S. Leroueil), pp. 2385-2409. London: Taylor and Francis.
- Holmes, D. M., Kumar, R. V. & Clegg, W. J. (2006). Cracking during lateral drying of alumina suspensions. *J. Am. Ceram. Soc.*, **89**, No. 6, 1908-1913.
- Jain, A. K. & Juanes, R. (2008). Pore-scale mechanistic study of the preferential mode of hydrate formation in sediments: Coupling of multiphase fluid flow and sediment mechanics. *Proc. 6th Int. Conf. Gas Hydrates (ICGH 2008)*, Vancouver, British Columbia, Canada.
- Koliji, A., Laloui, L., Cusinier, O. & Vulliet, L. (2006). Suction induced effects on the fabric of a structured soil. *Transp. Porous Media* **64**, No. 2, 261-278.
- Konrad, J. M. & Ayad, R. (1997). An idealized framework for the

- analysis of cohesive soils undergoing desiccation. *Can. Geotech. J.* **34**, No. 4, 477–488.
- Lachenbruch, A. H. (1962). *Mechanics of thermal contraction cracks and ice-wedge polygons in permafrost*, No. 70. New York: Geological Society of America.
- Lu, N., Wu, B. & Tan, C. P. (2007). Tensile strength characteristics of unsaturated sands. *J. Geotech. Geoenviron. Engng* **133**, No. 2, 144–154.
- Lura, P., Pease, B., Mazzotta, G. B., Rajabipour, F. & Weiss, J. (2007). Influence of shrinkage-reducing admixtures on development of plastic shrinkage cracks. *ACI Mater. J.* **104**, No. 2, 187–194.
- Morris, P. H., Graham, J. & Williams, D. J. (1992). Cracking in drying soils. *Can. Geotech. J.* **29**, No. 2, 263–277.
- Naser Abu-Hejleh, A. & Znidarcic, D. (1995). Desiccation theory for soft cohesive soils. *J. Geotech. Engng* **121**, No. 6, 493–502.
- Palomino, A. M. & Santamarina, J. C. (2005). Fabric map for kaolinite: Effects of pH and ionic concentration on behavior. *Clays Clay Miner.* **53**, No. 3, 211–223.
- Peng, X. & Horn, R. (2007). Anisotropic shrinkage and swelling of some organic and inorganic soils. *Eur. J. Soil Sci.* **58**, No. 1, 98–107.
- Prodanovic, M. & Bryant, S. L. (2006). A level set method for determining critical curvatures for drainage and imbibition. *J. Colloid Interface Sci.* **304**, No. 2, 442–458.
- Rodriguez, R., Sanchez, M., Ledesma, A. & Lloret, A. (2007). Experimental and numerical analysis of desiccation of a mining waste. *Can. Geotech. J.* **44**, No. 6, 644–658.
- Sanford, R. J. (2003). *Principles of fracture mechanics*. Upper Saddle River, New Jersey: Prentice-Hall.
- Scherer, G. W. (1990). Theory of drying. *J. Am. Ceram. Soc.* **73**, No. 1, 3–14.
- Thusyanthan, N. I., Take, W. A., Madabhushi, S. P. G. & Bolton, M. D. (2007). Crack initiation in clay observed in beam bending. *Geotechnique*, **57**, No. 7, 581–594, doi: 10.1680/geot.2007.57.7.581.
- Towner, G. D. (1988). The influence of sand- and silt-size particles on the cracking during drying of small clay-dominated aggregates. *J. Soil Sci.* **39**, No. 3, 347–356.
- van Damme, H. & Ben Ohoud, M. (1990). From flow to fracture and fragmentation in colloidal media: 2, Local order and fragmentation geometry. In *Disorder and fracture* (eds J. C. Charmet, E. Guyon & S. Roux), pp. 105–116. New York: Plenum.
- Wang, Y. H. & Xu, D. (2007). Dual porosity and secondary consolidation. *J. Geotech. Geoenviron. Engng* **133**, No. 7, 793–801.
- Weinberger, R. (1999). Initiation and growth of cracks during desiccation of stratified muddy sediments. *J. Struct. Geol.* **21**, No. 4, 379–386.
- Wilson, G. W., Fredlund, D. G. & Barbour, S. L. (1997). Effect of soil suction on evaporative fluxes from soil surfaces. *Can. Geotech. J.* **34**, No. 1, 145–155.
- Zabat, M., Vayer-Besançon, M., Harba, R., Bonnamy, S. & Van Damme, H. (1997). Surface topography and mechanical properties of smectite films. In *Progress in colloid and polymer science* (eds J. B. Rosenholm, B. Lindman & P. Stenius), pp. 96–102. Berlin: Springer.
- Zarzycki, J., Prassas, M. & Phalippou, J. (1982). Synthesis of glasses from gels: The problem of monolithic gels. *J. Mater. Sci.* **17**, No. 11, 3371–3379.